Acta Cryst. (1995). B51, 952–961

Phase Transition Upon d^{10} Cd^{2+} Ordering in $CdPS_3$

BY F. BOUCHER, M. EVAIN* AND R. BREC

IMN, Laboratoire de Chimie des Solides, UMR CNRS No. 110, Université de Nantes, 2 rue de la Houssinière, 44072 Nantes CEDEX 03, France

(*Received* 13 *January* 1995; *accepted* 5 *April* 1995)

Abstract

A phase transition at *ca* 228 K in cadmium trithiophosphate, $CdPS_3$, has been characterized by means of single-crystal X-ray diffraction. The low-temperature phase crystallizes in trigonal symmetry [$a = 6.224(3)$, $c = 19.49(1)$ Å, $V = 654(1)$ Å^3 and $Z = 6$]. The structure determination was conducted from 679 reflections [$I \geq 2.5\sigma(I)$]. Several refinement procedures providing for stacking faults and nonharmonicity were conducted in the $R\bar{3}$ centrosymmetric and $R3$ noncentrosymmetric space groups. The best solution (23 variables, $R3$ space group, inversion center between two of the three domain types originating from the stacking faults) led to reliability factors of $R = 2.02$ and $wR = 2.28\%$. Apart from the stacking faults, the low-temperature structure of $CdPS_3$ essentially differs from the room-temperature form by the stacking mode (CdI_2 *versus* $CdCl_2$ type) on the one hand, and by the ordering of the Cd atoms on octahedral off-centered positions on the other. The Cd ordering and the stacking mode change are discussed in terms of electronic and steric stability, respectively.

1. Introduction

The MPX_3 phases (M = divalent transition metal and X = S or Se) form a large family of compounds first discovered by C. Friedel 100 years ago (Friedel, 1894). In the last decades numerous physical and chemical studies were initiated on these compounds, in particular several structural analyses (Klingen, Eulenberger & Hahn, 1968; Klingen, 1969; Klingen, Eulenberger & Hahn, 1970; Klingen, Eulenberger & Hahn, 1973; Klingen, Ott & Hahn, 1973; Carpentier & Nitsche, 1974; Jandali, Eulenberger & Hahn, 1978; Wiedenmann, Rossat-Mignod, Louisy, Brec & Rouxel, 1981; Brec, Louisy, Ouvrard, Verbaere & Rouxel, 1982; Ouvrard, Brec & Rouxel, 1985; Prouzet, Ouvrard & Brec, 1986). Basically, they have shown that the thio- and selenophosphates can be considered as layered materials of the CdI_2 or $CdCl_2$ types in which, within the layer, one third of the transition metals M are substituted by P_2 pairs.

The extent of research performed on those MPX_3 phases allowed Brec *et al.* (Brec, Ouvrard & Rouxel, 1985) to establish certain trends, especially between the structural parameters and the physical and chemical properties. For instance, a relation between the atomic displacement parameters (ADP's) of the transition metals and their electronic configuration was clearly demonstrated. Indeed, cations with a d^5 or d^{10} spherical electronic configuration such as Mn^{2+}, Zn^{2+} or Cd^{2+} have unusually high ADP's compared with other elements (Fe^{2+}, Co^{2+}, Ni^{2+} *etc.*). The idea of a low ligand field stabilization was then proposed to explain the anomalous behavior.

A vibrational study (Barj, Lucazeau, Ouvrard & Brec, 1988) on three elements of the family ($MnPS_3$, $NiPS_3$ and $CdPS_3$) then showed, through a valence force-field (VFF) calculation, that high Cd^{2+} ADP's were generated by a positional disorder and not by a purely vibrational disorder. This was recently confirmed (Boucher, Evain & Brec, 1994) in a study from single-crystal X-ray data of the nonharmonic behavior of the cadmium site potential. The probability density function (p.d.f.), the characteristic function of the displacement factor (commonly known as the temperature factor), of the Cd atom splits into two maxima, the signature of a positional disorder. The lack of stabilization of the ligand field ascribable to a spherical electronic configuration alone cannot explain the difference in ADP's between d^5 and d^{10} cations (Barj, Lucazeau, Ouvrard & Brec, 1988). Thus, a second-order Jahn–Teller effect (Jahn & Teller, 1937) was thought to be responsible for the difference. Such a phenomenon implying a mixing upon distortion between occupied nd and unoccupied $(n + 1)s$ orbitals is indeed observed for Ag^+ and Cu^+ ions and can account for positional disorders (Burdett & Eisenstein, 1992). However, in the case of cadmium, a possible hybridization is questionable because of the rather wide energy gap between the nd and $(n + 1)s$ levels that could be too large to allow for a sufficient energy lowering (Orgel, 1958; Jorgensen, 1957).

The original aim of the study was the evolution of the p.d.f. at the cadmium site. Indeed, upon lowering the temperature the vibrational amplitudes decline, which in turn makes the positional disorder detection easier. It is worth noting that, at room temperature, the Cd splitting shown by means of a development of the displacement factor (Boucher, Evain & Brec, 1994) was unexpectedly observed in the direction of an octahedron

* Author to whom correspondence should be addressed.

ISSN 0108-7681

Table 1. *Experimental details*

	$R\bar{3}$	$R3$
Crystal data		
Chemical formula	$CdPS_3$	$CdPS_3$
Chemical formula weight	239.6	239.6
Cell setting	Trigonal	Trigonal
Space group	$R\bar{3}$ (hexagonal axes)	$R3$ (hexagonal axes)
a (Å)	6.224 (3)	6.224 (3)
b (Å)	6.224 (3)	6.224 (3)
c (Å)	19.49 (1)	19.49 (1)
α (°)	90.0	90.0
β (°)	90.0	90.0
γ (°)	120.0	120.0
V (Å^3)	654 (1)	654 (1)
Z	6	6
D_x (Mg m^{-3})	3.649	3.649
Radiation type	Mo K-$L_{2,3}$	Mo K-$L_{2,3}$
Wavelength (Å)	0.71073	0.71073
No. of reflections for cell parameters	24	24
θ range (°)	1–40	1–40
μ (mm^{-1})	6.531	6.531
Temperature (K)	133	133
Crystal form	Platelet	Platelet
Crystal size (mm)	0.0012 × 0.0012 × 0.0012	0.0012 × 0.0012 × 0.0012
Crystal color	Colorless	Colorless
Data Collection		
Diffractometer	Siemens $P4$	Siemens $P4$
Monochromator	Oriented graphite (002)	Oriented graphite (002)
Data collection method	ω scans	ω scans
Absorption correction	Gaussian	Gaussian
T_{min}	0.485	0.485
T_{max}	0.720	0.720
No. of measured reflections	3256	3256
No. of independent reflections	914	914
No. of observed reflections	679	679
Criterion for observed reflections	$I > 2.5\sigma(I)$	$I > 2.5\sigma(I)$
R_{int}	0.032	0.032
θ_{max} (°)	40	40
Range of h, k, l	$-1 \rightarrow h \rightarrow 11$ $-11 \rightarrow k \rightarrow 10$ $-35 \rightarrow l \rightarrow 35$	$-1 \rightarrow h \rightarrow 11$ $-11 \rightarrow k \rightarrow 10$ $-35 \rightarrow l \rightarrow 35$
No. of standard reflections	3	3
Frequency of standard reflections	Every 100 reflections	Every 100 reflections
Intensity decay (%)	<0.1	<0.1
Refinement		
Refinement on	F	F
R*	0.019	0.020
wR†	0.021	0.023
S‡	1.27	1.34
No. of reflections used in refinement	679	679
No. of parameters used (M)	36	23
Weighting scheme	$w = [\sigma^2\|F_O\| + (0.01\|F_O\|)^2]^{-1}$	$w = [\sigma^2\|F_O\| + (0.01\|F_O\|)^2]^{-1}$
$(\Delta/\sigma)_{max}$	0.003	0.006
$\Delta\rho_{max}$ (e Å^{-3})	0.6	0.7
$\Delta\rho_{min}$ (e Å^{-3})	−0.6	−0.8
Extinction method	Type I Gaussian (Becker & Coppens, 1974)	Type I Gaussian (Becker & Coppens, 1974)
Extinction coefficient§	3.1 (3) × 10^{-6}	3.1 (3) × 10^{-6}
Source of atomic scattering factors	Cromer & Waber (1974) and Cromer (1974)	Cromer & Waber (1974) and Cromer (1974)

* $R = \Sigma||F_o| - |F_c||/\Sigma|F_o|$.
† $wR = [\Sigma w(|F_o| - |F_c|)^2/\Sigma w|F_o|^2]^{1/2}$.
‡ $S = [\Sigma w(|F_o| - |F_c|)^2/(N - M)]^{1/2} (N = 679)$.
§ Isotropic secondary extinction.

edge, along the monoclinic b axis. A more favorable direction, such as that perpendicular to the sandwich, which coincides with the major density elongation, was clearly anticipated. However, this last splitting could have been masked by the overall high thermal motion (Bachmann & Schulz, 1984). One purpose of the low-temperature study was then an improvement of the disorder resolution to unravel the enigma. In addition, it was of interest to check Lifshitz *et al.*'s (Lifshitz, Francis & Clarke, 1983) observation of a first-order transition at *ca* 260 K for this compound, although no clear-cut evidence of that transition could be obtained from differential scanning calorimetry measurements. In this paper we report the atomic structure of the low-temperature ordered form of $CdPS_3$, illustrating the d^{10} Cd^{2+} ordering.

Table 2. *Atomic and displacement parameters; $R\bar{3}$ hypothesis*

$B_{eq} = (8\pi^2/3)\sum_i \sum_j U_{ij} a_i^* a_j^* \mathbf{a}_i.\mathbf{a}_j$.

Atom	Cd1	Cd2	P1	P2	P3	S	Atom	S
τ	0.8034 (8)	0.3932	0.6068	0.1966	0.1966	1	C111	−0.0007 (6)
x	0	2/3	2/3	0	0	0.3391 (1)	C222	−0.0016 (6)
y	0	1/3	1/3	0	0	0.3294 (1)	C333	0.00000 (1)
z	0.33092 (2)	1/3	0.39050 (6)	0.2755 (2)	0.3896 (2)	0.41983 (4)	C112	0.0017 (4)
B_{eq}	0.996 (5)	1.14 (2)	0.50 (1)	0.66 (5)	0.61 (5)	1.10 (1)	C113	0.00010 (9)
U_{11}	0.00788 (8)	0.0079 (2)	0.0065 (2)	0.0074 (7)	0.0061 (6)	0.0149 (2)	C122	−0.0022 (4)
U_{22}	U_{11}	U_{11}	U_{11}	U_{11}	U_{11}	0.0152 (2)	C123	−0.00005 (7)
U_{33}	0.0221 (1)	0.0275 (4)	0.0061 (4)	0.010 (1)	0.011 (1)	0.0099 (1)	C133	−0.00003 (3)
U_{12}	$(1/2)U_{11}$	$(1/2)U_{11}$	$(1/2)U_{11}$	$(1/2)U_{11}$	$(1/2)U_{11}$	0.0063 (1)	C223	−0.00005 (9)
U_{13}	0	0	0	0	0	0.0006 (1)	C233	0.00007 (3)
U_{23}	0	0	0	0	0	0.0000 (1)		

τ represents the occupation ratio of the position.
The expression of the harmonic displacement factor is $\exp(-2\pi^2 \sum_i \sum_j U_{ij} a_i^* a_j^* h_i h_j)$, with U_{ij} in Å^2.
Third-order tensor elements C_{pqr} are multiplied by 10^3.

2. Experimental

$CdPS_3$ was obtained from heating the constituent elements in stoichiometric proportions (1:1:3) in an evacuated silica tube. A 983 K temperature was maintained for 1 week for a good crystal yield. A single crystal of suitable shape and quality was selected and subsequently tested with the usual rotation and Weissenberg techniques. In expectation of the low-temperature measurements, the crystal was glued at the tip of a quartz Lindemann capillary using a Torr Seal vacuum sealing kit. The data collection was performed on a Siemens *P*4 diffractometer (Euler geometry, Mo K-$L_{2,3}$ radiation, and graphite monochromator). A first set of intensities was collected at room temperature to validate our crystal choice and absorption correction by comparison with known results. In total, 2777 reflections were measured within one half of the diffraction sphere ($-h/h$, $-k/k$, $0/l$) in the 1–40° (θ) range. After the conventional Lorentz–polarization and absorption (Gaussian integration) corrections, equivalent reflections were averaged according to the $2/m$ Laue class yielding the internal consistency R_{int} value of 1.6%. A set of 1109 reflections with $I > 2.5\sigma(I)$ was then left for refinement. Applying the nonharmonic refinement procedure previously used by Boucher *et al.* (Boucher, Evain & Brec, 1994), acceptable reliability factors (R = 2.10 and wR = 2.44%) were reached, confirming the good quality of the selected crystal.

For the low-temperature measurement, a Siemens LT-2A attachment mounted on the chi-circle directly opposite the crystal mount was used (nitrogen gas temperature tightly regulated by a thermocouple and frost prevented by a surrounding warm dry gas and a heated deflector). A 123 K set-point temperature was chosen to reach an effective temperature of *ca* 133 K at the sample level.

A phase transition, as suggested by Lifshitz *et al.* (Lifshitz, Francis & Clarke, 1983), although quite different in nature (*vide infra*), was observed upon cooling. The transition occurs at 228 K and deeply affects the system lattice. With monoclinic C centered at room temperature, the symmetry shifts to trigonal at the transition. The transformation matrix from the monoclinic [a_M = 6.218 (1), b_M = 10.763 (2), c_M = 6.867 (1) Å and β = 107.58 (4)°] to the hexagonal parameter set used to describe the rhombohedral cell [a_H = 6.224 (3) and c_H = 19.49 (1) Å] is

$$\begin{pmatrix} a_H \\ b_H \\ c_H \end{pmatrix} = \begin{pmatrix} -1 & 0 & 0 \\ \frac{1}{2} & \frac{1}{2} & 0 \\ -1 & 0 & -3 \end{pmatrix} \begin{pmatrix} a_M \\ b_M \\ c_M \end{pmatrix}.$$

Taking into account the R centering of the hexagonal cell, 3256 *hkl* lattice planes sweeping a half space of the diffraction sphere were explored (see Table 1). After the application of standard corrections (*vide supra*) and the averaging of equivalent planes according to the $R\bar{3}$ point symmetry (R_{int} = 3.2%), 679 independent reflections with $I > 2.5\sigma(I)$ could be used in the refinement. All calculations were carried out with the *SDS*95 program package (Petříček, 1995). The scattering factors for neutral atoms and the anomalous dispersion correction were taken from Cromer & Waber (1974) and Cromer (1974). All refinements were based on $|F_o|$ and performed in a full-matrix mode, using $w = 1/[\sigma^2|F_o| + (0.01|F_o|)^2]$ as weights.*

3. Refinement and structure analysis

3.1. $R\bar{3}$ *hypothesis*

3.1.1. *Refinement.* Browsing through published data, one easily sees that the MPX_3 structures adopt two different stacking patterns. One compound subset [$ZnPS_3$, $NiPS_3$, $MnPS_3$, $CoPS_3$ and $FePS_3$ (Ouvrard, Brec & Rouxel, 1985; Prouzet, Ouvrard & Brec, 1986)] is related to the $CdCl_2$ type (*ABC/ABC* stacking mode), while the other [$MgPSe_3$, $MnPSe_3$, $FePSe_3$ and $CdPSe_3$ (Klingen, 1969; Klingen, Eulenberger & Hahn, 1973;

*A list of structure factors has been deposited with the IUCr (Reference: DU0398). Copies may be obtained through The Managing Editor, International Union of Crystallography, 5 Abbey Square, Chester CH1 2HU, England.

Wiedenmann, Rossat-Mignod, Louisy, Brec & Rouxel, 1981)] is associated with the CdI_2 type (*AB/AB* stacking mode). Consequently, two different crystalline systems are found for the MPX_3 phases, a monoclinic and trigonal symmetry characterizing the $CdCl_2$ and CdI_2 structural type, respectively.

$CdPS_3$ seems a border compound since it adopts both crystalline systems. At room temperature the anion stacking is *ABC/ABC*, but below 228 K, given the rhombohedral observed cell, it should be *AB/AB*, similar to that of the $MPSe_3$ phases. With the knowledge of all previous studies, we started off our structure analysis within the $R\bar{3}$ centrosymmetric space group.

A structure factor normalization and the subsequent use of direct methods unravelled the atom localization, giving three positions (Cd1, P1 and S; see Table 2) compatible with known $MPSe_3$ arrangements. Refinements of such a solution yielded a rather high reliability *R* factor (30%). A difference-Fourier synthesis revealed important electronic density residues at the center of the P1–P1 pair and on both sides of the Cd1 atom. As demonstrated for other compounds [$V_{0.78}PS_3$ (Ouvrard, Fréour, Brec & Rouxel, 1985) and $CoPS_3$ (Ouvrard, Brec & Rouxel, 1985)], a cationic disorder was considered. It is worth noting that, at room temperature, the cation arrangement is perfectly ordered. Therefore, the disorder clearly results from stacking faults generated at the phase transition.

Thus, additional phosphorus (P2 and P3) and cadmium (Cd2) atoms (see Table 2) were introduced near the initial Cd1 position and in between the P1 atoms of the P1–P1 pair, respectively. Occupational ratios were determined and restricted according to the following rules: (1) a cationic site should be totally occupied either by a Cd atom or a P pair, and (2) the overall phase stoichiometry should be fulfilled. Hence, the Cd1 occupational ratio alone was set free, the other site occupation percentages being deduced through dependence relations.

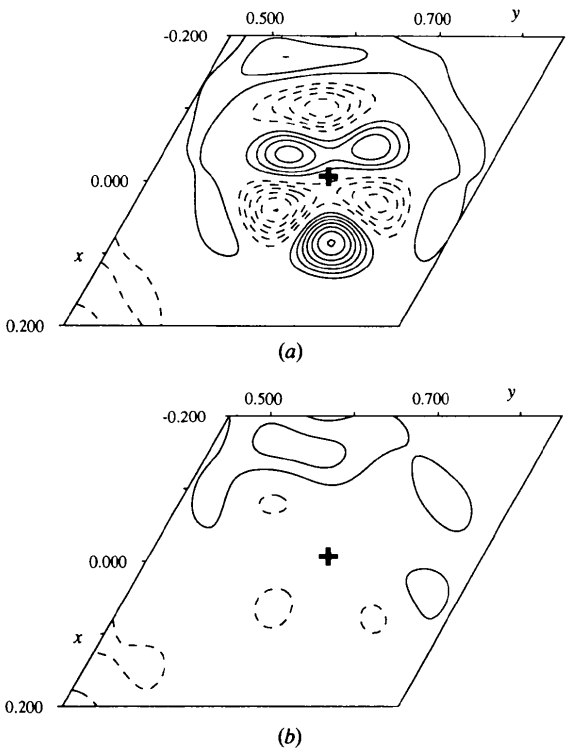

Fig. 1. Difference-Fourier map around the S mean position for low-temperature $CdPS_3$ ($R\bar{3}$ hypothesis): (*a*) harmonic refinement; (*b*) nonharmonic refinement. Both *xy* sections at $z = 0.42$. Contour lines from -1.2 to -0.2 e Å^{-3} (dashed lines) and from 0.2 to 1.4 e Å^{-3} (continuous lines) in intervals of 0.2 e Å^{-3}. S mean position indicated by +.

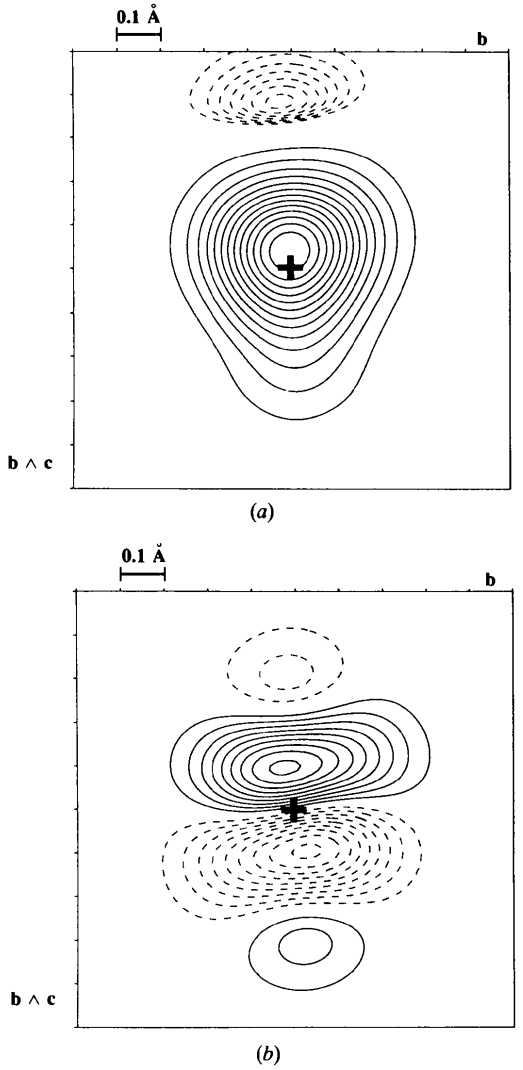

Fig. 2. (*a*) The *xy* section at $z = 0.42$ of the S nonharmonic p.d.f. for low-temperature $CdPS_3$. Contour lines from -350 to -50 Å^{-3} in intervals of 50 Å^{-3} (dashed lines) and from 2000 to 26 000 Å^{-3} (continuous lines) in intervals of 2000 Å^{-3}. S mean position indicated by +. (*b*) Nonharmonic deformation-density map (same section). Contour lines from -4500 to -500 Å^{-3} (dashed lines) and from 500 to 4500 Å^{-3} (continous lines) in intervals of 500 Å^{-3}. Maps are centered on the sulfur mean position.

Upon introducing the anisotropic ADP's, this hypothesis proved to dramatically lower the reliability factors (R = 2.44 and wR = 2.79%). Nevertheless, difference-Fourier syntheses still revealed significant residues in the sulfur position vicinity (see Fig. 1*a*). As a consequence of the stacking faults, a distribution of positions might exist at these locations and of course cannot be taken into account with a normal (harmonic) extension of the displacement factor. A positional disorder (static disorder) can be equivalently modeled by split positions or by a nonharmonic (high order) development of the displacement factor (Bachmann & Schulz, 1984), the latter being better since generating much less paramater correlations.

The introduction of third-order tensors in the Gram-Charlier expansion (Johnson & Levy, 1974) of the sulfur displacement factor greatly improved the modeling of the electronic density around the anionic site. With only ten additional parameters, the reliability factors dropped to R = 1.92 and wR = 2.14% and the major residues were lowered from +1.4 and −1.1 to $\pm 0.6\ e\ Å^{-3}$ (see Fig. 1*b*). According to the Hamilton test (Hamilton, 1965), this approach is satisfactory since to be conclusive the R value should only be lower than 2.39%. However, before having full confidence in that model, the physical meaning of the p.d.f. should be checked. The sulfur nonharmonic p.d.f. along with the nonharmonic deformation-density map (Kuhs, 1988) are given in Fig. 2. The nonharmonic contribution to the density function clearly maps the major residues left over by the harmonic model. In addition, given the low values of the p.d.f. negative regions (<1.3% of the maximum), the model can be considered as valid (Bachmann & Schulz, 1984) and well adapted to the description of the structure.

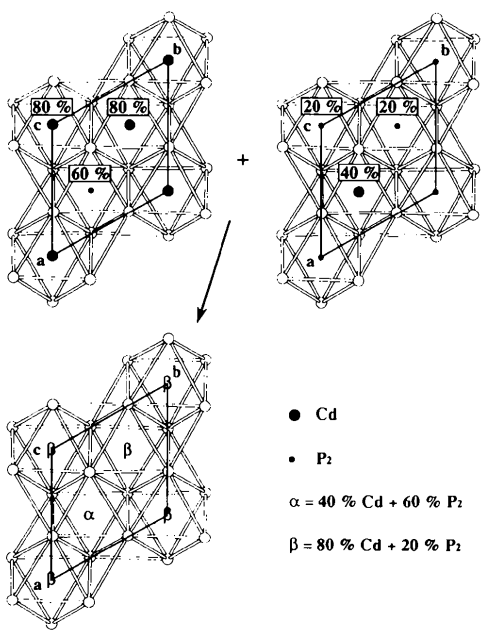

Fig. 3. Disordered low-temperature $CdPS_3$ layer (bottom) seen as the superposition of two cation fillings (top) leading to two nonequivalent cationic sites (α and β). $R\bar{3}$ hypothesis.

3.1.2. *Model analysis and discussion.* The cationic distribution obtained in the centrosymmetric space group approach is shown in Fig. 3. The figure presents both the major atomic contributions (Cd1 and P1; Fig. 3, top left) and the minor ones (Cd2, P2 and P3; Fig. 3, top right), the combination of the two giving the disordered pattern (Fig. 3, bottom left) observed at low temperature. On average, two different cationic sites are found: the α sites principally occupied by P2 pairs and the β sites mainly filled by Cd ions. Within a layer the β sites outnumber the α sites in a 2:1 ratio.

A thorough Cd—S* and P—S* distance analysis, using the mode position S* (0.3438, 0.3266, 0.41983), which is the maximum of the p.d.f. at the sulfur site, clearly shows a departure of the calculated bond distances from those expected from the room-temperature structure determination (see Table 3). If the apparent calculated P—S* and Cd—S* distances are close to the expected values when the element under scrutiny is preponderent (P1 in α sites and Cd1 in β sites, respectively), they differ from those expected values when the element is the minor component. For instance, the Cd2—S* distance [2.6073 (8) Å, β sites] is inexplicably shorter than the usual distance observed at room temperature [*e.g.* 2.7194 (7) Å in room-temperature $CdPS_3$]. More critical, the calculated average P—S distance (from P2—S* and P3—S*) is much larger [2.196 (1) Å] than the usual value of *ca* 2.03 Å [*e.g.* 2.0298 (8) Å in room-temperature $CdPS_3$], found to be quasi-invariant in the MPS_3 family. It is then obvious that, although beyond reproach as far as the refinement is concerned, the model is questionable since it yields unusual distances. The calculated distances obtained from the modes are physically meaningless because of the disorder. A new model, less symmetrical, leading to true distances was sought. The noncentrosymmetric $R3$ space group was indeed a good candidate.

3.2. *R3 hypothesis*

3.2.1. *Refinement.* The observed low-temperature disorder supposedly affects the stacking of the [$CdPS_3$] sandwiches and not the sandwich content. This hypothesis is based upon the fact that the room-temperature structure was perfectly ordered before the reversible phase transition and that cation site movements are very unlikely at such a temperature. To accurately describe the layers it is therefore possible to use a method similar to that of Evain *et al.* (Evain, Monconduit, van der Lee, Brec, Rouxel & Canadell, 1994) for the Ta_3SiTe_6 disordered phase. Indeed, in their approach one considers that each sandwich is fully ordered and that the apparent disorder within the sandwich is generated upon averaging several ordered domains. In $CdPS_3$, the disorder can easily be modeled by the existence of three domain types with different probabilities (the coherence

Table 3. *Main interatomic distances* (Å); $R\bar{3}$ *hypothesis*†

Cd1—S*	2.7136 (9)	(×3)	Cd2—S*	2.6073 (8)	(×6)
Cd1—S*	2.7033 (9)	(×3)			
Cd1—S^*_{av}	2.7085 (9)				
P1—S*	2.0694 (8)	(×3)	P1—P1	2.228 (2)	
P2—S*	2.221 (1)	(×3)	P2—P3	2.225 (5)	
P3—S*	2.170 (1)	(×3)			
P(2,3)—S^*_{av}	2.196 (1)				

† Calculations based upon the S* sulfur p.d.f. mode (0.3438, 0.3266, 0.41983).

length remaining quite long since no important intensity profile modification was observed). Such an approach considers that the sandwich atomic structure remains ideal away from any domain border and even at the stacking fault itself, since the influence of neighboring sandwiches on a given sandwich is regarded as very small. This is often a very good approximation for metallic close packings and compounds such as ZnS or SiC (Jagodzinsky & Frey, 1993). In the MPS_3 phases, the interactions between the sandwiches being of the van der Waals type, the sandwiches may very well be considered as undisturbed at the fault.

In a first stage, the three domain types were considered to be structurally linked through simple in-plane translations. This is schematized in Fig. 4. Type I domains (type I, ~60%) are obtained with the Cd1 and P1 sites of the previous model. The in-plane locations of the type II and III domains are deduced from type I domains by application of the $(1/3a_H + 2/3b_H)$ and $(2/3a_H + 1/3b_H)$ translations, respectively. With an appropriate stoichiometry for the latter domain types (~20% for each one), the combination of the three domain types gives a distribution identical to that of the $R\bar{3}$ hypothesis.

The atomic parameters were set free for the atoms attached to the type I domains only. The other atomic parameters were constrained to the free ones through the dependence relations, that is, a pseudocentering of the cell for the positions and an identity for the ADP's of related atoms (through the pseudocentering). To prevent too high correlations between the positional and the displacement parameters, atoms related by the inversion center in the $R\bar{3}$ hypothesis were assumed to present the same ADP's. An obvious relation between the three domain types ratio ascertaining the overall stoichiometry was established

$$\tau(\mathrm{I}) + \tau(\mathrm{II}) + \tau(\mathrm{III}) = 1.$$

In addition, since the percentages of type II and III domains were related (correlation coefficient of −1.0 *vide infra*), they were constrained to the same value. Therefore, τ(II) and τ(III) were linked to τ(I) through the relation

$$\tau(\mathrm{II}) = \tau(\mathrm{III}) = (1/2)[1 - \tau(\mathrm{I})].$$

With 679 *hkl*'s and 22 parameters, the confidence factors converged to the values R = 2.13 and wR = 2.48%. The residues in the difference-Fourier synthesis then ranged from +0.75 to −1.0 e Å^{-3}. However, the convergence was very slow due to very high correlation coefficients [*e.g.* 0.995 between x(S1) and x(S2) and between y(S1) and y(S2)]. Also, the relation established between τ(II) and τ(III) could not be justified. This led us to a second refinement strategy.

In this second stage, type III domains are not linked to type I domains by the $(\frac{2}{3}a_H + \frac{1}{3}b_H)$ pseudotranslation, but to type II domains by an inversion center at $(\frac{1}{6}, \frac{1}{3}, \frac{1}{3})$ (symmetry element of the $R\bar{3}$ space group, fixing the origin in the $R3$ space group). The centrosymmetric (or close to centrosymmetric) nature of the average structure (*vide supra*) naturally introduce the percentage constraint established between type II and III domains, type I domains being close to centrosymmetric alone.

Without any dampening factors, the refinement smoothly converged to the confidence factors R = 2.02 and wR = 2.28% for 23 variables. Slight improvements were observed on the difference-Fourier maps, with the extrema lowered to +0.7 and −0.8 e Å^{-3}. A final check of the modeling of the sulfur disorder was nevertheless necessary. Taking into account the complete set of sulfur atomic parameters describing the overall

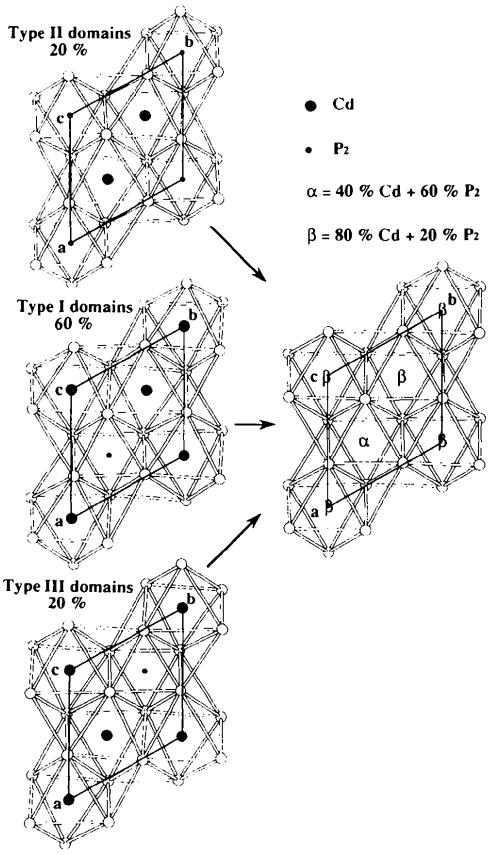

Fig. 4. Disordered low-temperature $CdPS_3$ layer (left) build up from three ordered domain sets (right) yielding the same two nonequivalent cationic sites as in Fig. 3. $R3$ hypothesis.

Table 4. *Atomic and displacement parameters; R3 hypothesis*

Atom	Cd1	Cd2	P1	P2	S1	S2
x	0	1/3	2/3	2/3	0.3450 (3)	−0.0168 (3)
y	0	2/3	1/3	1/3	0.3214 (3)	0.3422 (3)
z	0.3291 (1)	0.33798 (5)	0.3900 (1)	0.2757 (1)	0.4201 (2)	0.2471 (2)
B_{eq}	0.856 (7)	0.856	0.54 (1)	0.54	0.65 (1)	0.65
U_{11}		0.00792 (7)		0.0065 (2)		0.0087 (2)
U_{22}		U_{11}		U_{11}		0.0100 (2)
U_{33}		0.0167 (2)		0.072 (3)		0.0099 (1)
U_{12}		$(1/2)U_{11}$		$(1/2)U_{11}$		0.0077 (1)
U_{13}		0		0		0.0011 (4)
U_{23}		0		0		0.0005 (4)
Domain I (%)				60.96 (8)		
Domain II (%)				19.52		
Domain III (%)				19.52		

The atomic parameters are given for domain I.

Domain II is deduced from I by the translation $\frac{1}{3}a_H + \frac{2}{3}b_H$ and domain III is related to II by an inversion center at $(\frac{1}{6}, \frac{1}{3}, \frac{1}{3})$.

See also notes in Table 2.

Table 5. *Main interatomic distances* (Å) *and angles* (°); *R3 hypothesis**

		$Cd1S_6$ site			
Cd1—S1	2.733 (3)	(×3)	$(S1—S1)_{//}$	3.599 (3)	(×3)
Cd1—S2	2.707 (3)	(×3)	$(S2—S2)_{//}$	3.783 (3)	(×3)
$Cd1—S_{av}$	2.720 (3)				
$(S1—Cd1—S1)_{cis}$	82.4 (1)	(×3)			
$(S2—Cd1—S2)_{cis}$	88.7 (1)	(×3)			
		$Cd2S_6$ site			
Cd2—S1	2.710 (3)	(×3)	$(S1—S1)_{//}$	3.787 (4)	(×3)
Cd2—S2	2.751 (3)	(×3)	$(S2—S2)_{//}$	3.644 (3)	(×3)
$Cd2—S_{av}$	2.730 (3)				
$(S1—Cd2—S1)_{cis}$	88.7 (1)	(×3)			
$(S2—Cd2—S2)_{cis}$	83.0 (1)	(×3)			
		P_2S_6 site			
P1—P2	2.227 (3)		$(S1—S1)_{//}$	3.405 (3)	(×3)
P1—S1	2.052 (2)	(×3)	$(S2—S2)_{//}$	3.365 (3)	(×3)
P2—S2	2.022 (2)	(×3)			
$P—S_{av}$	2.037 (2)				
(S1—P1—S1)	112.1 (1)	(×3)			
(S2—P2—S2)	112.7 (1)	(×3)			
		Through the van der waals gap			
S1—S2	3.746 (4)	S1—S2	3.754 (4)	S1—S2	3.763 (4)

* // indicates a distance in the *A* (or *B*) sulfur planes.

structure (two positions per domain type), the joint p.d.f. map (Bachmann & Schulz, 1984; see Fig. 5) matches reasonably well that of the $R\bar{3}$ hypothesis (see Fig. 2).

Of the two domain descriptive approaches, the second gives the best results, both in terms of convergence and residues. It was therefore chosen as the final structural model. Atomic positions, ADP's and occupation ratios are gathered in Table 4.

3.2.2. *Model analysis and discussion.* Firstly, the relative proportion of the domain types is in good agreement with that of the $R\bar{3}$ hypothesis. Indeed, the P_2 (Cd) occupation ratio of the α (β) type sites is 60.96 (8)% [80.5 (1)] in the latter description to be compared with 60.7 (1)% [80.34 (6)] in the former approach. The domain model proves the most effective for the disorder description: (1) interatomic distances (see Table 5) do not depart much from room-temperature calculated values [*e.g.* 2.037 (2) Å for the P—S distance against 2.0298 (8) Å]; (2) meaningful equivalent ADP's are now calculated [*i.e.* 0.856 (7), 0.54 (1) and 0.65 (1) $Å^2$ for Cd, P and S, respectively]; (3) a discussion of the atomic arrangement within a fully ordered sandwich is made possible. It should be pointed out that a twinning could not be considered because of the structure factor phase coherence.

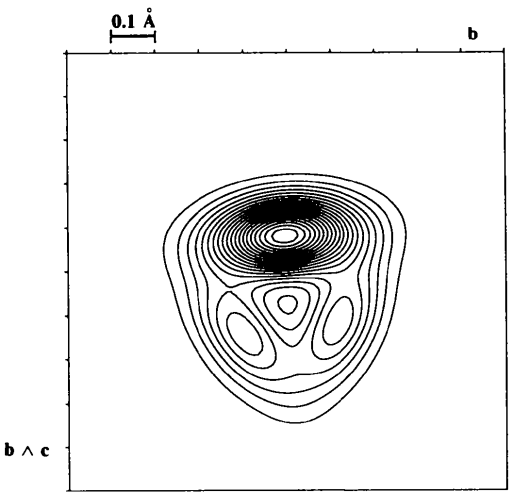

Fig. 5. The *xy* section at $z = 0.42$ of the S harmonic joint p.d.f. for low-temperature $CdPS_3$ (*R*3 hypothesis), including the six S contributions (two per domain type). The overall shape matches reasonably well that of the $R\bar{3}$ hypothesis presented in Fig. 2. Contour lines from 2000 to 40 000 $Å^{-3}$ in intervals of 2000 $Å^{-3}$.

4. Discussion

From $CdPS_3$ single-crystal X-ray diffraction analyses on films and manganese-doped $CdPS_3$ EPR studies, Lifshitz *et al.* (Lifshitz, Francis & Clarke, 1983) tentatively characterized the $CdPS_3$ phase transition. They evidenced a first-order transition occurring around 260 K with a coexistence of both phases over a 16 K temperature range. Although displaced toward 228 K in our analysis, as shown by the evolution of two strong reflections presented in Fig. 6, the transition is confirmed. Its first-order character is also proved since no subgroup-to-group relation exists between *R*3 and *C*2/*m* space groups. In addition, a 17° modification of the β monoclinic angle at the transition, implying an alteration of the anion close stacking, was reported. From a Weissenberg analysis, it was concluded that an orthorhombic symmetry for low-temperature $CdPS_3$ be assigned, which was used for the EPR interpretation. Our studies validate the stacking modification but contradict the symmetry deduction. One possible source of error that could have misled Lifshitz *et al.* could be the orientation of the crystal at room temperature, the C-centered orthohexagonal cell of the MPS_3 phases being directly related to an hexagonal cell (Ouvrard & Brec, 1990).

The temperature dependence of the lattice parameters obtained from the selected single crystal and calculated from 26 high-angle ($21.2 < 2\theta < 38.3°$) strong reflection positions is presented in Fig. 7. For a better understanding of the cell evolution, only relevant dimensions have been reported, *i.e.* the a parameter common to both systems and the $\frac{1}{3}c_H$ and $c_M \sin b_M$ stacking 'periodicities'. The graph clearly shows that the system metric mostly evolves not within the layer plane but along the stacking direction. The a parameter hardly changes at the transition, in agreement with the minor modification within the sandwich (which incidentally validates our hypothesis of an unchanged slab structure). On the contrary, the stacking mode change from *ABC/ABC* to *AB/AB* results in a discontinuity of the stacking parameter. From a macroscopic point of view, the effect primarily affects the van der Waals gap. The intersandwich spacing shrinks from 3.18 Å at room temperature to 3.12 Å at low temperature, whereas the sandwich thickness barely increases (3.36 Å at room temperature against 3.37 Å at low temperature). A close examination of the S—S distances across the van der Waals gap points to a steric effect as the origin of the discontinuity. Indeed, at low temperature the S—S distances are homogeneous [3.746 (4)–3.763 (3) Å, average 3.754 (4) Å], but at room temperature they spread over a wide range [3.7179 (9)–3.8704 (7) Å, average 3.8015 (9) Å]. Therefore, the adjustment of the anion layers at the van der Waals gap is better at low than at room temperature and the packing more compact.

In agreement with our out-of-plane splitting expectation (*vide supra*), our current analysis shows an ordering of the cadmium cations onto two off-centered positions, along the trigonal threefold axis, towards the van der Waal gap. Upon ordering, the CdS_6 octahedra undergo a strong distortion. To visualize that distortion, the main Cd—S distances and S—Cd—S *cis* angles at the cadmium site in room-temperature $CdPS_3$ and low-temperature $CdPS_3$ are presented in Fig. 8. The off-centered Cd positions (±0.09 Å) largely modify the octahedra geometry, although keeping the Cd—S distances homogeneous and similar to the room-temperature calculated distances. When the Cd atom approaches the van der Waals gap, the sulfur triangle swells, with the S—S distance increasing from 3.70 (room temperature) to 3.78 Å. On the contrary, the facing sulfur triangle shrinks. This distortion can also be observed on the S—Cd—S octahedron *cis* angles, which increase or decrease by *ca* 3°. It is worth noting that the P_2S_6 group remains almost unchanged in the ordering process.

The question of the influence of the Cd ordering on the stacking mode modification should be addressed. Could the anion layer shift be induced by a steric energy gain or by an electronic process through across-the-gap interactions? To tentatively answer that question, a hypothetical $CdPS_3$ structure was built from the low-temperature [$CdPS_3$] sandwich, but with the room-temperature *ABC/ABC* stacking mode (rather than the *AB/AB* observed). The chosen lattice unit was the ideal monoclinic C-centered cell deduced from the low-temperature lattice parameters with the proper transformation matrix (*vide supra*). In this way, the low-temperature average S—S distance across the van der Waals gap could be reproduced (3.754 Å). A thorough analysis of the S—S distances then shows an enhancement of the disparity (3.623–3.878 Å). Therefore, it seems that the *ABC/ABC* mode becomes less favorable than the *AB/AB* mode upon distortion of the CdS_6 octahedra.

In the previous room-temperature study (Boucher, Evain & Brec, 1994) we argued that the density splitting could be due to a second-order Jahn–Teller effect, implying a mixing on distortion between occupied *nd* and unoccupied $(n + 1)s$ orbitals (*vide supra*). A recent *ab initio* band structure calculation (Zhukov,

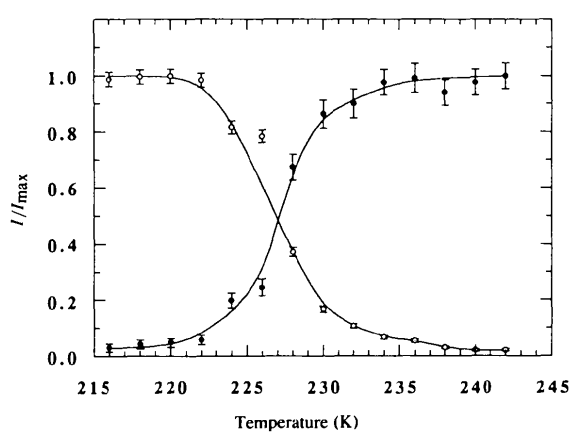

Fig. 6. Phase transition shown as the evolution of two reflection intensities *versus* temperature in the {213, 243}K range: room-temperature monoclinic $\bar{1}32$ reflection in filled circles and low-temperature rhombohedral $\bar{1}23$ reflection in open circles. Error bars chosen as 3σ.

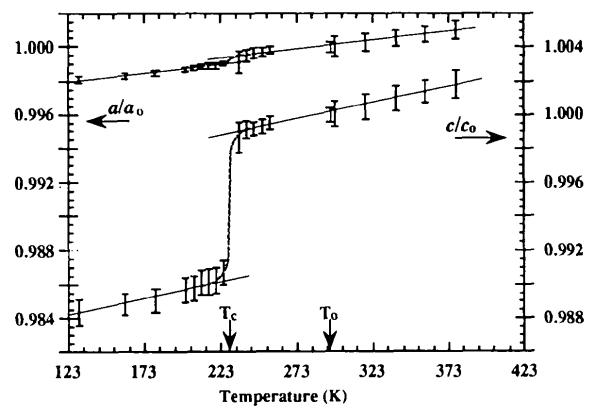

Fig. 7. Cell-parameter variation as a function of temperature. The a/a_0 parameter ratio common to both systems and the c/c_0 stacking periodicity ratio (c and c_0 redefined as $\frac{1}{3}c_H$ or $c_M \sin b_M$). Subscripts o and c represent room- and transition-temperature values. Error bars taken as 3σ.

Boucher, Alemany, Evain & Alvarez, 1995) indicates that the origin of the cadmium displacement is indeed a second-order Jahn–Teller stabilization, but this stabilization results not from an $nd - (n + 1)s$ hybridization but from a mixing of the Cd p and $P_2S_6^{4-}$ $1e_g$ orbitals. No direct relation between the stacking mode change and the second-order Jahn–Teller effect could be found. The low-temperature trigonal form is calculated to be more stable than the room-temperature monoclinic form by 0.3 eV (per unit cell), but this energy gain cannot result from the hybridization only since a shift of 0.1 Å of the cadmium ions would generate a gain not larger than 0.05 eV. These new findings reinforce the idea that the relative stabilization of both stacking modes results from a complex interplay between the layers, taking into account van der Waals forces, short-range repulsions and HOMO/LUMO interactions.

Our investigations, in particular the cell-parameter variation study, have shown the importance of the steric interaction at the van der Waals gap and the influence of the anion layer distortion on the stacking. In a previous MPS_3 survey, Ouvrard *et al.* (Ouvrard & Brec, 1990) stated that it is possible to use X-ray powder-pattern-refined cell parameters to determine the amplitude and nature of any stacking distortion in MPS_3. They clearly mixed up the system metric and the motif. Considering the metric only (obtained from X-ray powder pattern), room-temperature $CdPS_3$ anion stacking seems as regular [b/a ratio close to the ideal $3^{1/2}$ value and β almost equal to $\cos^{-1}(-a/3c)$] as the low-temperature arrangement (trigonal symmetry). Only a close look at the local distances (motif consideration) shows the real stacking perfectness or distortion. A departure of the parameters from the ideal values probably points to stacking distortions, but nothing can be said when these parameters perfectly match the ideal values.

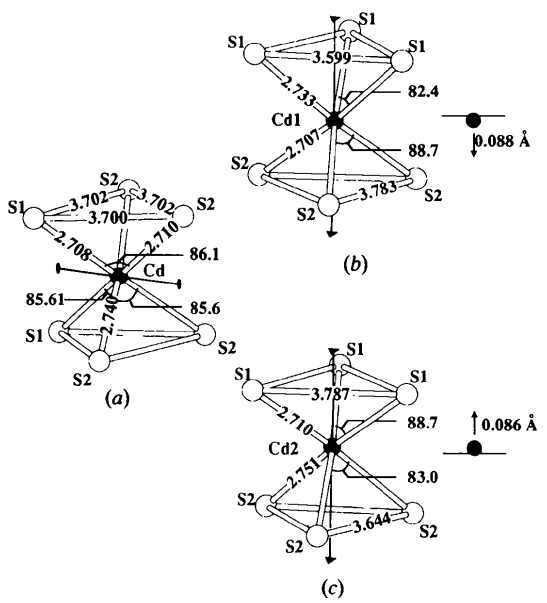

Fig. 8. Distances (Å) and *cis* angles (°) in the octahedral site of $CdPS_3$ for (*a*) room temperature, (*b*) low-temperature Cd1 and (*c*) low-temperature Cd2. The Cd off-centered displacement in the ordered low-temperature phase is underlined.

5. Concluding remarks

In this study we have reported the structural analysis of low-temperature $CdPS_3$ and the d^{10} cation ordering. Using a domain approach we have been able to pinpoint the true nature of the low-temperature $CdPS_3$ slab and therefore to observe fine structural details that would have been biased in a conventional approach (split model). This information provides new insights on the stability of d^{10} Cd^{2+} in an octahedral environment on the one hand and of $CdCl_2$ and CdI_2 stacking modes on the other hand.

References

BACHMANN, R. & SCHULZ, H. (1984). *Acta Cryst.* A**40**, 668–675.

BARJ, M., LUCAZEAU, G., OUVRARD, G. & BREC, R. (1988). *Eur. J. Solid State Inorg. Chem.* **25**, 449–461.

BECKER, P. J. & COPPENS, P. (1974). *Acta Cryst.* A**30**, 129–147.

BOUCHER, F., EVAIN, M. & BREC, R. (1994). *J. Alloys Compd*, **215**, 63–70.

BREC, R., LOUISY, A., OUVRARD, G., VERBAERE, A. & ROUXEL, J. (1982). *Rev. Chim. Miner.* **19**, 49–57.

BREC, R., OUVRARD, G. & ROUXEL, J. (1985). *Mat. Res. Bull.* **20**, 1257–1263.

BURDETT, J. K. & EISENSTEIN, O. (1992). *Inorg. Chem.* **31**, 1758–1762.

CARPENTIER, C. D. & NITSCHE, R. (1974). *Mat. Res. Bull.* **9**, 401–410.

CROMER, D. T. (1974). *International Tables for X-ray Crystallography*, edited by J. A. IBERS & W. C. HAMILTON, Vol. IV, pp. 149–150. Birmingham: Kynoch Press.

CROMER, D. T. & WABER J. T. (1974). *International Tables for X-ray Crystallography*, edited by J. A. IBERS & W. C. HAMILTON, Vol. IV, pp. 72–98. Birmingham: Kynoch Press.

EVAIN, M., MONCONDUIT, L., VAN DER LEE, A., BREC, R., ROUXEL, J. & CANADELL, E. (1994). *New J. Chem.* **18**, 215–222.

FRIEDEL, C. (1894). *C. R.* **119**, 260–264.

HAMILTON, W. (1965). *Acta Cryst.* **18**, 502–510.

JAGODZINSKY, H. & FREY, F. (1993). *International Tables for X-ray Crystallography*, edited by U. SHMUELI, Vol. B, pp. 406–411. Dordrecht: Kluwer Academic Publishers.

JAHN, H. A. & TELLER, E. (1937). *Proc. R. Soc. A*, **161**, 220–235.

JANDALI, M. Z., EULENBERGER, G. & HAHN, H. (1978). *Z. Anorg. Allg. Chem.* **447**, 105–118.

JOHNSON, C. K. & LEVY, H. A. (1974). *International Tables for X-ray Crystallography*, edited by J. A. IBERS & W. C. HAMILTON, Vol. IV, pp. 311–336. Birmingham: Kynoch Press.

JORGENSEN, C. K. (1957). PhD Thesis, Copenhagen Univ.

KLINGEN, W. (1969). PhD Thesis, Höhenheim Univ.

KLINGEN, W., EULENBERGER, G. & HAHN, H. (1968). *Naturwissenschaften*, **55**, 229–230.

KLINGEN, W., EULENBERGER, G. & HAHN, H. (1970). *Naturwissenschaften*, **57**, 88.

KLINGEN, W., EULENBERGER, G. & HAHN, H. (1973). *Z. Anorg. Allg. Chem.* **401**, 97–112.

KLINGEN, W., OTT, R. & HAHN, H. (1973). *Z. Anorg. Allg. Chem.* **396**, 271–278.

KUHS, W. F. (1988). *Aust. J. Phys.* **41**, 369–382.

LIFSHITZ, E., FRANCIS, A. H. & CLARKE, R. (1983). *Solid State Commun.* **45**, 273–276.

ORGEL, L. E. (1958). *J. Chem. Soc.* pp. 4186–4190.
OUVRARD, G. & BREC, R. (1990). *Eur. J. Solid State Inorg. Chem.* **27**, 477–488.
OUVRARD, G., BREC, R. & ROUXEL, J. (1985). *Mat. Res. Bull.* **20**, 1181–1189.
OUVRARD, G., FRÉOUR, R., BREC, R. & ROUXEL, J. (1985). *Mat. Res. Bull.* **20**, 1053–1062.
PETŘÍČEK, V. (1995). *SDS95*. Institute of Physics, Praha, Czech Republic.
PROUZET, E., OUVRARD, G. & BREC, R. (1986). *Mat. Res. Bull.* **21**, 195–200.
WIEDENMANN, A., ROSSAT-MIGNOD, J., LOUISY, A., BREC, R. & ROUXEL, J. (1981). *Solid State Commun.* **40**, 1067–1072.
ZHUKOV, V., BOUCHER, F., ALEMANY, P., EVAIN, M. & ALVAREZ, S. (1995). *Inorg. Chem.* In the press.

Acta Cryst. (1995). B**51**, 961–972

X-ray and Neutron Diffuse Scattering in $LiNbO_3$ from 38 to 1200 K

BY N. ZOTOV,† F. FREY, H. BOYSEN, H. LEHNERT, A. HORNSTEINER AND B. STRAUSS

Institut für Kristallographie und Mineralogie, Universität München, Theresienstrasse 41, 80333 *München, Germany*

R. SONNTAG, H. M. MAYER AND F. GÜTHOFF

Hahn–Meitner Institut, BENSC, Glienickerstrasse 100, 14109 *Berlin, Germany*

AND D. HOHLWEIN

Institut für Kristallographie, Universität Tübingen c/o Hahn–Meitner Institut, Glienickerstrasse 100, 14109 *Berlin, Germany*

(*Received* 4 *November* 1994; *accepted* 23 *March* 1995)

Abstract

A semi-quantitative description of X-ray and neutron diffuse scattering from *congruent* lithium niobate, $LiNbO_3$, is given. The diffuse scattering is concentrated in three sets of diffuse planes perpendicular to the pseudo-cubic symmetry-related [221], [241] and $[4\bar{2}1]$ directions and can be attributed to one-dimensional displacive and chemical disorder along these directions. The variation of the X-ray and neutron diffuse intensities with the scattering vector, as well as the comparison between X-ray and neutron data, indicate that more than one type of atom is involved. Temperature variations are followed from 38 to 1200 K. Different disorder models are discussed. The increase of the integrated intensities of the diffuse lines along the $[0\,1k\,2l]^*$ and $[0\,\bar{1}k\,4l]^*$ directions (*i.e.* sections of the diffuse planes) up to 800 K followed by a slight decrease at higher temperatures may be interpreted either by static disorder related to temperature-dependent variation of disorder/defect clusters or by dynamic disorder. Inelastic neutron scattering experiments do not show any anomaly of the transversal acoustic (TA) modes.

1. Introduction

After the discovery of the ferroelectric properties of lithium niobate ($LiNbO_3$), its average structure has been extensively studied (Abrahams, Reddy & Bernstein, 1966; Abrahams, Hamilton & Reddy, 1966; Abrahams & Marsh, 1986; Iyi *et al.*, 1992; Boysen & Altorfer, 1994; Zotov, Boysen, Frey, Metzger & Born, 1994). Lithium niobate (denoted LN hereafter) melts incongruently. Its structure and physical properties depend strongly on the Li:Nb ratio (Räuber, 1978) and can be substantially changed by small amounts of dopant ions. It is therefore important to understand the defects and the corresponding defect structures. Different models have been discussed in the literature (Lerner, Legras & Dumas, 1968; Nassau & Lines, 1970; Bollmann & Gernand, 1972; Peterson & Carnevale, 1972; Donnerberg, Tomlinson, Catlow & Schirmer, 1989; Schirmer, Thiemann & Wöhlecke, 1991; Metzger, 1993). All these models represent short-range order arrangements of a small number of vacancies around the Nb_{Li} (Nb on Li sites) atoms, including ilmenite-type defects. However, none have been confirmed experimentally.

Direct information about the real structure can be obtained by measurement of the diffuse scattering. X-ray diffuse scattering from LN and $LiTaO_3$ was first reported

† On leave from the Institute of Applied Mineralogy, Rakovskistreet 92, Sofia 1000, Bulgaria.